passing them over a neutral alumina column prior to use in order to remove any peroxides or inhibitors present. 4-Nitrostyrene was prepared in two stages by nitrating (β-bromoethyl)benzene with fuming nitric acid to yield a mixture of 2- and 4-nitro-(β-bromoethyl)benzene. The 4-nitro-(β-bromoethyl)benzene was then purified by crystallization from heptane (yield 60%). The 4-nitro-(β-bromoethyl)benzene dissolved in toluene was then treated with an excess of 50% NaOH in the presence of polyethylene glycol 400 as catalyst[35] at room temperature which after crystallization from hexane gave 4-nitrostyrene (mp 29 °C, yield 90%, purity GLC 99%). Iodosobenzene was prepared by the common literature method.[36]

The following research instruments were used: atomic absorption, GBC 603 single beam spectrometer; UV-vis, Hewlett Packard 8452 diode parray spectrometer; FTIR, Analect FX 6260; ESR, Brucker ESP300; GLC, Hewlett Packard 5890 equipped with an FID detector, a Model 3396 integrator, and 10-m cross-linked FFAP megabore column (i.d. 0.53 mm with a 1.0 μm coating); GC-MS, Hewlett Packard 5970 A with a mass selective detector; cyclic voltammetry, BAS CV-IB voltammograph with a glassy carbon working electrode and a Ag/AgCl reference electrode.

Preparation of $SiRu(H_2O)W_{11}O_{39}^{5-}$. $K_5SiRu(H_2O)W_{11}O_{39}$ was prepared by first dissolving 1.0 mmol of $K_8SiW_{11}O_{39}$[22] in 100 mL of water at 80 °C. After the unsaturated heteropolyanion was completely dissolved (about 30 min) 1.05 mmol of $RuCl_3 \cdot H_2O$ dissolved in a small amount of water was slowly added, and the mixture was stirred at 90 °C for 30 min. The solution was cooled to 50 °C, and 80 mL of methanol was added which precipitated a brown-black sticky solid. The solid was filtered at the pump and then was twice titurated with acetone to yield the black crystalline $K_5SiRu(H_2O)W_{11}O_{39}$ with a 70% yield. The ruthenium heteropolyanion was analyzed by using atomic absorption to determine potassium and ruthenium[37] and gravimetric analysis for Si and W as SiO_2[38] and the 8-hydroxyquindinotungstate,[39] respectively. Water of hydration was found by thermogravimetric analysis. The analysis yields the molecular formula $K_5SiRu(H_2O)W_{11}O_{39} \cdot 15H_2O$, and the calculated (found) percentages are K, 6.00 (6.04); Si, 0.86 (0.73); Ru, 3.10 (3.01); W, 62.05 (60.82); H_2O, 8.84 (8.52).

$((C_6H_{13})_4N)_5SiRu^{III}(H_2O)W_{11}O_{39}$ was prepared by vigorously mixing 0.5 mmol of $K_5SiRu^{III}(H_2O)W_{11}O_{39}$ dissolved in 20 mL of water with 2.6 mmol of $(C_6H_{13})_4NHSO_4$ in 30 mL of dichloromethane. After the ruthenium heteropolyanion was entirely transferred into the organic phase, phases were separated, the organic phase was dried with $MgSO_4$, and the solvent was removed yielding a crystalline $((C_6H_{13})_4N)_5SiRu^{III}(H_2O)W_{11}O_{39}$ in a 95% yield. The calculated (found) percentages for the organic counter cation are C, 30.68 (30.29); H, 5.72 (5.48); N, 1.54 (1.28).

Typical Procedure for the Oxidatin of Olefins. Reactions were performed in a 25-mL flask equipped with a thermostated oil bath and a magnetic stirrer. Thus 0.002 mmol of $((C_6H_{13})_4N)_5SiRu^{III}(H_2O)W_{11}O_{39}$ and 1.0 mmol of substrate in 5 mL of 1,2-dichloroethane were mixed with 5 mmol of oxidant at 60 ± 2 °C. The oxidants were added in 5 mL of water in the case of sodium periodate and potassium persulfate, as a solid in the case of iodosobenzene and as a liquid in the case of *tert*-butyl hydroperoxide (technical grade 70%). Samples were taken at the appropriate intervals and analyzed by GLC. Peaks were standardized by using the available reference compounds.

(35) Kimura, Y.; Regen, S. L. *J. Org. Chem.* **1983**, *48*, 195.
(36) Saltzman, H.; Sharefkin, J. F. *Org. Synth.* **1960**, *43*, 60.
(37) Rowston, W. B.; Ottaway, J. M. *Anal. Lett.* **1970**, *3*, 411.
(38) Erdey, L. *Gravimetric Analysis Part III*; Pergamon Press: Oxford, 1965; p 185.
(39) Erdey, L. *Gravimetric Analysis Part II*; Pergamon Press: Oxford, 1965; p 550.

Models for Diferrous Forms of Iron-Oxo Proteins. Structure and Properties of $[Fe_2BPMP(O_2CR)_2]BPh_4$ Complexes

A. S. Borovik,[†] M. P. Hendrich,[‡] T. R. Holman,[†] E. Münck,*[,‡] V. Papaefthymiou,[‡] and L. Que, Jr.*[,†]

Contribution from the Department of Chemistry, University of Minnesota, Minneapolis, Minnesota 55455, and Gray Freshwater Biological Institute, University of Minnesota, Navarre, Minnesota 55392. *Received January 23, 1990*

Abstract: A series of bimetallic complexes, $[M^{II}M'^{II}BPMP(O_2CR)_2]X_2$ where BPMP is the anion of 2,6-bis[[bis(2-pyridylmethyl)amino]methyl]-4-methylphenol, has been synthesized to serve as models for the diferrous forms of iron-oxo centers in proteins. Complex **1** (M = M′ = Fe, R = C_2H_5, X = BPh_4, solvate = 0.8 CH_2Cl_2) has been characterized by X-ray diffraction methods as having a (μ-phenoxo)bis(μ-carboxylato)diiron core. **1** crystallizes in the triclinic space group $P\bar{1}$ with cell constants: a = 12.607 (6) Å, b = 15.113 (13) Å, c = 16.601 (6) Å, α = 81.42 (6)°, β = 88.88 (4)°, γ = 67.89 (5)°, Z = 2, V = 2879.4 Å^3. From 11 192 reflections (of 13 865 where I(obsd) > $\sigma(I)$) collected at 175 K, the structure was solved by the Patterson method and refined anisotropically to R = 0.058 and R_w = 0.074. The metal centers in **1** have distinct six-coordinate environments but have similar structural parameters. They have been characterized as high-spin Fe(II) centers by electronic spectral, NMR, Mössbauer, and EPR methods with the help of the analogous heterobimetallic complexes such as the $Fe^{II}Zn^{II}$ and $Fe^{II}Ga^{III}$ derivatives. Most interestingly, **1** and **2** (M = M′ = Fe, R = Ph, X = BPh_4) exhibit low field EPR signals near **g** = 16, similar to those reported for deoxyhemerythrin azide, reduced methane monooxygenase and reduced ribonucleotide reductase. The signal for **1** has an intensity that is enhanced in parallel mode ($\mathbf{B}_1 \parallel \mathbf{B}$), a characteristic of integer spin systems, and has a temperature dependence indicative of a ground-state transition. Analysis of EPR spectra shows that the two iron sites of **1** are ferromagnetically coupled. Depending on the sign of the zero-field splitting parameters D_i of the individual Fe(II) sites, both a weak and a strong coupling scheme are compatible with the data. Similar but significantly less intense signals are observed for analogous $Fe^{II}Zn^{II}$ or $Fe^{II}Ga^{III}$ complexes, as expected for the **S** = 2 centers in these complexes.

In recent years, dinuclear iron-oxo centers have emerged as a common structural component in the active sites of several metalloproteins.[1] These centers have important functional roles in hemerythrin,[2] ribonucleotide reductase,[3] methane monooxygenase,[4] and the purple acid phosphatases.[5] The prototype and best characterized member of this class of proteins is hemerythrin (Hr),

[†] Department of Chemistry.
[‡] Gray Freshwater Biological Institute.

(1) (a) Que, L., Jr.; Scarrow, R. C. In *Metal Clusters in Proteins*; Que, L., Jr., Ed.; ACS Symposium Series 372; American Chemical Society: Washington, DC, 1988; pp 159-178. (b) Lippard, S. J. *Angew. Chem., Int. Ed. Engl.* **1988**, *27*, 344-361.

0002-7863/90/1512-6031$02.50/0

a respiratory protein found in some marine invertebrates. In particular, the $Fe^{III}Fe^{III}$ form has been shown by crystallographic and spectroscopic studies to have a (μ-oxo)bis(μ-carboxylato)diiron core.[1,2,6] This structure has been reproduced in synthetic $Fe^{III}Fe^{III}$ complexes by spontaneous self-assembly methods, thus illustrating the thermodynamic stability of this triply bridged dinuclear unit.[7] Diiron complexes of this type have served as excellent models for the structural and spectroscopic properties of the oxidized form of dinuclear iron proteins.

The coordination chemistry of the diiron centers in the diferrous oxidation state is less well understood. Such centers can be found in reduced forms of hemerythrin,[8,9] methane monooxygenase,[10] and ribonucleotide reductase[11,12] and have been shown or postulated to be involved in dioxygen binding and/or activation chemistry. For deoxyHr a variety of physical measurements suggest that the triply bridged unit is retained, with the oxo group being protonated to give a (μ-hydroxo)bis(μ-carboxylato)diiron(II,II) core.[1,8b,9] This bridging arrangement apparently results in weak antiferromagnetic coupling between the ferrous centers (J = 30 cm^{-1} for $\mathcal{H} = JS_1 \cdot S_2$) and the EPR silence of the complex.[9,13] The addition of azide, however, elicits a novel low field EPR signal, which is proposed to arise from the $|\pm 4\rangle$ levels of a ferromagnetically coupled diferrous system (S = 4) on the basis of MCD studies.[9] Similar low field signals have been found for the diferrous forms of methane monooxygenase[10a] and *E. coli* ribonucleotide reductase B2 subunit.[11]

We have undertaken an effort to model these diferrous sites to enhance our understanding of their properties. The only compound thus far that has a structurally characterized (μ-hydroxo)bis(μ-carboxylato)diiron(II,II) core is $[Fe_2(Me_3TACN)_2(OH)(OAc)_2]X$[14] reported by Wieghardt et al.,[15] which features antiferromagnetically coupled ferrous centers (J = 26 cm^{-1}) and is thus EPR-silent. More recently, Lippard et al.[16] have reported the synthesis of another diferrous complex $[Fe_2(BIPhMe)_2(HCO_2)_4]$, with a μ-O,O-formato bridge in place of the hydroxo bridge in the diiron core. We have approached the synthesis of such $Fe^{II}Fe^{II}$ complexes by using the dinucleating ligand 2,6-bis[[bis(2-pyridylmethyl)amino]methyl]-4-methylphenol, HBPMP, which provides a phenolate in place of the bridging hydroxide.[18] Unlike the (μ-hydroxo)diiron(II) complex, the (μ-formato) and (μ-phenoxo) derivatives exhibit low field EPR signals[16,17] which are found for several of the dinuclear iron-oxo proteins in their diferrous oxidation states. The spectroscopic properties of the BPMP complexes are reported in this paper. The availability of the heterobimetallic $Fe^{II}Ga^{III}$ and $Fe^{II}Zn^{II}$ derivatives substantially enhances our understanding of the $Fe(II)_2$ complexes by allowing the properties of an individual Fe(II) center to be studied in an environment similar to that in the $Fe(II)_2$ complex but without the metal–metal coupling interaction. A preliminary account of the crystal structure of the diferrous bis(propionate) derivative and its properties has been published.[17]

Table I. The Crystallographic Experiments and Computations[a] for **1**

formula	$C_{64}H_{65}BCl_2Fe_2N_6O_5$
formula wt, amu	1191.7
temp, K	175
crystal system	triclinic
space group	$P\bar{1}$
a, Å	12.607 (6)
b, Å	15.113 (13)
c, Å	16.601 (6)
α, deg	81.42 (6)
β, deg	88.88 (4)
γ, deg	67.89 (5)
V, Å^3	2879
Z	2
D(calc), g cm^{-3}	1.37
crystal dim, mm	0.25 × 0.50 × 0.35
radiation	Mo Kα (λ = 0.7107 Å)
monochromator	graphite
μ, cm^{-1}	4.26
scan type	ω
2θ range, deg	4–50
indices collected	$+h,\pm k,\pm l$
reflections	13865
	11192 used ($I > \sigma(I)$)
no. least sq param	467
data/parameters	24.0
R^b	0.058
$R_w{}^b$	0.073
GOF	1.880
p^a	0.05

[a] The intensity data were processed as described in the following: *CAD4 and SDP-PLUS User's Manual*; B.A. Frenz & Assoc.; College Station, TX, 1982. The net intensity $I = [K(NPI)](C - 2B)$, where K = 20.1166 (attenuator factor), NPI = ratio of fastest possible scan rate to scan rate for the measurement, C = total count, and B = total background count. The standard deviation in the net intensity is given by $[\sigma(I)]^2 = (k/NPI)^2[C + 4B + (pI)^2]$ where p is a factor used to downweight intense reflections. The observed structure factor amplitude F_o is given by $F_o = (I/Lp)^{1/2}$, where Lp = Lorentz and polarization factors. The $\sigma(I)$'s were converted to the estimated errors in the relative structure factors $\sigma(F_o)$ by $\sigma(F_o) = {}^1/_2[\sigma(I)/I]F_o$. [b] $R = (\sum||F_o| - |F_c||)/(\sum F_o)$; $R_w = \{(\sum w|F_o - F_c|^2)/(\sum w(F_o)^2)\}^{1/2}$; GOF = $\{(\sum w(|F_o| - |F_c|)^2)/(N_{data} - N_{params})\}^{1/2}$.

Experimental Section

All reagents and solvents were purchased from commercial sources and used as received, unless noted otherwise. The following solvents were distilled under nitrogen before use: methanol from $Mg(OCH_3)_2$ and acetonitrile from CaH_2. Microanalyses were performed by Desert Analytics, Inc., Tuscon, AZ. The ligand, 2,6-bis[[bis(2-pyridylmethyl)amino]methyl]-4-methylphenol (HBPMP), was synthesized according to published procedures.[18b]

(2) Wilkins, P. C.; Wilkins, R. G. *Coord. Chem. Rev.* **1987**, *79*, 195–214.
(3) Reichard, P.; Ehrenberg, A. *Science (Washington, D.C.)* **1983**, *221*, 514–519.
(4) (a) Woodland, M. P.; Patil, D. S.; Cammack, R.; Dalton, H. *Biochim. Biophys. Acta* **1986**, *873*, 237–242. (b) Prince, R. C.; George, G. N.; Savas, J. C.; Cramer, S. P.; Patel, R. N. *Biochim. Biophys. Acta* **1988**, *952*, 220–229. (c) Ericson, A.; Hedman, B.; Hodgson, K. O.; Green, J.; Dalton, H.; Bentsen, J. G.; Beer, R. H.; Lippard, S. J. *J. Am. Chem. Soc.* **1988**, *110*, 2330–2332. (d) Fox, B. G.; Surerus, K. K.; Münck, E.; Lipscomb, J. D. *J. Biol. Chem.* **1988**, *263*, 10553–10556.
(5) (a) Antanaitis, B. C.; Aisen, P. *Adv. Inorg. Biochem.* **1983**, *5*, 111–136. (b) Averill, B. A.; Davis, J. C.; Burman, S.; Zirino, T.; Sanders-Loehr, J.; Loehr, T. M.; Sage, J. T.; Debrunner, P. G. *J. Am. Chem. Soc.* **1987**, *109*, 3760–3767.
(6) (a) Stenkamp, R. E.; Sieker, L. C.; Jensen, L. H. *J. Am. Chem. Soc.* **1984**, *106*, 618–622. (b) Sheriff, S.; Hendrickson, W. A.; Smith, J. L. *J. Mol. Biol.* **1987**, *197*, 273–296.
(7) (a) Armstrong, W. H.; Spool, A.; Papaefthymiou, G. C.; Frankel, R. B.; Lippard, S. J. *J. Am. Chem. Soc.* **1984**, *106*, 3653–3667. (b) Wieghardt, K.; Pohl, K.; Gebert, W. *Angew. Chem., Int. Ed. Engl.* **1983**, *22*, 727–728. (c) Spool, A.; Williams, I. D.; Lippard, S. J. *Inorg. Chem.* **1985**, *24*, 2156–2162. (d) Toftlund, H.; Murray, K. S.; Zwack, P. R.; Taylor, L. F.; Anderson, O. P. *J. Chem. Soc., Chem. Commun.* **1986**, 191–193. (e) Gomez-Romero, P.; Casan-Pator, N.; Ben-Hussein, A.; Jameson, G. *J. Am. Chem. Soc.* **1988**, *110*, 1988–1990.
(8) (a) Stenkamp, R. E.; Sieker, L. C.; Jensen, L. H.; McCallum, J. D.; Sanders-Loehr, J. *Proc. Natl. Acad. Sci. U.S.A.* **1985**, *82*, 713–716. (b) Zhang, K.; Stern, E. A.; Ellis, F.; Sanders-Loehr, J.; Shiemke, A. K. *Biochemistry* **1988**, *27*, 7470–7479.
(9) (a) Reem, R. C.; Solomon, E. I. *J. Am. Chem. Soc.* **1984**, *106*, 8323–8325. (b) Reem, R. C.; Solomon, E. I. *J. Am. Chem. Soc.* **1987**, *109*, 1216–1226.
(10) (a) Fox, B. G.; Surerus, K. K.; Münck, E.; Lipscomb, J. D. *J. Biol. Chem.* **1988**, *263*, 10553–10556. (b) Fox, B. G.; Froland, W. A.; Dege, J. E.; Lipscomb, J. D. *J. Biol. Chem.* **1989**, *264*, 10023–10033.
(11) (a) Lynch, J. B.; Juarez-Garcia, C.; Münck, E.; Que, L., Jr. *J. Biol. Chem.* **1989**, *264*, 8091–8096. (b) Hendrich, M. P.; Lynch, J. B. Unpublished results.
(12) Sahlin, M.; Graslünd, A.; Petersson, L.; Ehrenberg, A.; Sjöberg, B.-M. *Biochemistry* **1989**, *28*, 2618–2625.
(13) Maroney, M. J.; Kurtz, D. M., Jr.; Nocek, J. M.; Pearce, L. L.; Que, L., Jr. *J. Am. Chem. Soc.* **1986**, *108*, 6871–6879.
(14) Abbreviations used: Me_3TACN, 1,4,7-trimethyl-1,4,7-triazacyclononane; BIPhMe, 2,2′-bis(1-methylimidazolyl)phenylmethoxymethane; HBPMP, 2,6-bis[[bis(2-pyridylmethyl)amino]methyl]-4-methylphenol; HXTA, *N,N′*-2-hydroxy-5-methyl-1,3-xylylenebis(*N*-carboxymethylglycine).
(15) (a) Chaudhuri, P.; Wieghardt, K.; Nuber, B.; Weiss, J. *Angew. Chem., Int. Ed. Engl.* **1985**, *24*, 778–779. (b) Hartman, J. R.; Rardin, R. L.; Chaudhuri, P.; Pohl, K.; Wieghardt, K.; Nuber, B.; Weiss, J.; Papaefthymiou, G. C.; Frankel, R. B.; Lippard, S. J. *J. Am. Chem. Soc.* **1987**, *109*, 7387–7396.
(16) Tolman, W. B.; Bino, A.; Lippard, S. J. *J. Am. Chem. Soc.* **1989**, *111*, 8522–8523.
(17) Borovik, A. S.; Que, L., Jr. *J. Am. Chem. Soc.* **1988**, *110*, 2345–2347.

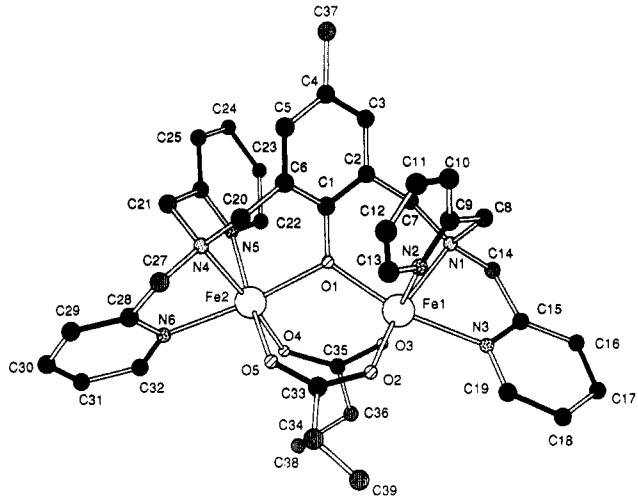

Figure 1. Plot of the complex cation of **1**, $[Fe_2BPMP(OPr)_2]^+$, with the numbering scheme.

(Bis-μ-*O*,*O*'-propionato)(2,6-bis[[bis(2-pyridylmethyl)amino]methyl]-4-methylphenolato)diiron(II,II) Tetraphenylborate, $[Fe^{II}_2BPMP(OPr)_2](BPh_4)\cdot 0.8CH_2Cl_2$ (1). A solution of 0.25 g (0.47 mmol) of HBPMP in 5 mL of methanol was treated under N_2 with a solution of 0.32 g (0.94 mmol) of $Fe(BF_4)_2\cdot 6H_2O$ in 10 mL of methanol. The resulting tan solution was treated with 0.14 g (1.4 mmol) of sodium propionate in 5 mL of methanol, thereby forming an orange-yellow solution. Metathesis with sodium tetraphenylborate (0.25 g, 0.73 mmol) resulted in the immediate precipation of the crude product. Further purification was achieved by recrystallization of the crude product by vapor diffusion of acetone into a dichloromethane solution of **1** to afford orange crystals of **1** (75% yield). Diffraction quality crystals were obtained by layering acetone over a dichloromethane solution of **1**; these crystals contained 0.8 of a molecule of occluded dichloromethane, which could be observed in the ^1H NMR of the complex. Anal. Calcd for $C_{63.8}H_{64.6}BCl_{1.6}Fe_2N_6O_5$ (**1**): C, 65.22; H, 5.55; N, 7.15. Found: C, 65.18; H, 5.60; N, 6.88.

(Bis-μ-*O*,*O*'-benzoato)(2,6-bis[[bis(2-pyridylmethyl)amino]methyl]-4-methylphenolato)diiron(II,II) Tetraphenylborate, $[Fe^{II}_2BPMP(OBz)_2]BPh_4\cdot 0.8CH_2Cl_2$ (2). This complex was prepared by using the same experimental procedure outlined for **1**, with sodium benzoate in place of sodium propionate. **2** was recrystallized from CH_2Cl_2/CH_3CN by vapor diffusion (68% yield). Anal. Calcd for $C_{72}H_{65}BCl_2Fe_2N_6O_5$ (**2**): C, 67.16; H, 5.09; N, 6.53. Found: C, 67.01; H, 4.95; N, 6.50.

(Bis-μ-*O*,*O*'-propionato)(2,6-bis[[bis(2-pyridylmethyl)amino]methyl]-4-methylphenolato)iron(II)zinc(II) Tetraphenylborate, $[Fe^{II}Zn^{II}BPMP(OPr)_2]BPh_4$ (3). This complex was prepared by adding 1.1 equiv of cobaltocene to a solution of $[Fe^{III}Zn^{II}BPMP(OPr)_2](BPh_4)_2$[19] (0.05 gm, 0.034 mmol) in 5 mL of CH_3CN under anaerobic conditions. The purple solution rapidly changed to yellow orange in color, indicating that reduction of the complex had occurred. Upon standing, a yellow precipitate appeared; this was filtered and recrystallized from CH_2Cl_2/CH_3CN to yield light orange crystals (0.027 gm, 66% yield). NMR studies of the complex indicate the presence of about 5% of the $Fe(II)_2$ and $Zn(II)_2$ complexes because of scrambling during the recrystallization process.

(Bis-μ-*O*,*O*'-propionato)(2,6-bis[[bis(2-pyridylmethyl)amino]methyl]-4-methylphenolato)iron(II)gallium(III) Bis(tetraphenylborate), $[Fe^{II}Ga^{III}BPMP(OPr)_2](BPh_4)_2\cdot CH_3COCH_3$ (4). This complex was prepared as reported previously.[19] Anal. Calcd for $C_{90}H_{89}B_2FeGaN_6O_6$ (**4**): C, 72.16; H, 6.00; N, 5.61. Found: C, 71.99; H, 6.01; N, 5.60.

Crystallographic Results for $[Fe^{II}_2(BPMP)(OPr)_2]BPh_4\cdot 0.8CH_2Cl_2$, 1. A crystal of **1** was mounted on an Enraf-Nonius CAD4 diffractometer. Crystal data, together with details of the diffraction experiment and subsequent calculations, are listed in Table I. The cell dimensions were obtained by least-squares refinement of the setting angles for 25 reflections (2θ = 15–36°). The stability of the crystal was monitored during data collection by measuring the intensities of three control reflections after every 4000 s of exposure time. No significant trend in these intensities was observed during the course of data acquisition. Lorentz and polarization corrections were applied to the data, and absorption corrections based on ψ scans were carried out (correction factors 0.975–1.000).

The structure was solved by using Patterson and Fourier methods. Neutral atom scattering factors (including anomalous scattering) were used.[20] All non-H atoms were refined with anisotropic thermal parameters. Hydrogen atoms were included in calculated positions (C–H = 0.95 Å, B_H = 3.0). Weighted ($w = [\sigma^2(R) + gF^2]^{-1}$) least-squares

Table II. Selected Bond Lengths (Å) and Angles (deg) for **1**[a]

	a. Bond Lengths		
Fe1–O1	2.062 (1)	Fe2–O1	2.052 (1)
Fe1–O2	2.035 (2)	Fe2–O4	2.045 (2)
Fe1–O3	2.150 (2)	Fe2–O5	2.138 (2)
Fe1–N1	2.259 (2)	Fe2–N4	2.250 (2)
Fe1–N2	2.232 (2)	Fe2–N5	2.241 (2)
Fe1–N3	2.165 (2)	Fe2–N6	2.178 (2)
O1–C1	1.338 (2)	O2–C33	1.266 (3)
O3–C35	1.246 (3)	O4–C35	1.276 (3)
O5–C33	1.249 (3)	N1–C7	1.494 (2)
N2–C9	1.346 (3)	N1–C8	1.472 (3)
N2–C13	1.344 (3)	N1–C14	1.478 (3)
N3–C15	1.346 (3)	N3–C19	1.339 (3)
N4–C20	1.493 (3)	N5–C22	1.344 (2)
N4–C21	1.483 (3)	N5–C26	1.343 (2)
N4–C27	1.474 (2)	N6–C28	1.341 (3)
N6–C32	1.350 (3)	C1–C2	1.407 (3)
C1–C6	1.400 (3)	C3–C4	1.393 (3)
C2–C3	1.396 (3)	C4–C5	1.390 (3)
C2–C7	1.503 (3)	C4–C37	1.515 (3)
C5–C6	1.396 (3)	C6–C20	1.505 (3)
C8–C9	1.511 (3)	C9–C10	1.390 (3)
C10–C11	1.372 (4)	C11–C12	1.389 (4)
C12–C13	1.383 (3)	C14–C15	1.510 (3)
C15–C16	1.377 (3)	C16–C17	1.384 (3)
C17–C18	1.385 (3)	C18–C19	1.384 (3)
C21–C26	1.508 (3)	C22–C23	1.380 (3)
C23–C24	1.382 (3)	C24–C25	1.380 (3)
C25–C26	1.399 (3)	C27–C28	1.512 (3)
C28–C29	1.396 (3)	C29–C30	1.389 (3)
C30–C31	1.384 (3)	C31–C32	1.387 (3)
C33–C34	1.511 (3)	C35–C36	1.523 (3)
C34–C38	1.394 (7)	C34–C38′	1.295 (9)
C36–C39	1.399 (5)	C36–C39′	1.22 (1)
Fe1–Fe2	3.348 (2)		
	b. Bond Angles (deg)		
O1–Fe1–O2	104.01 (6)	O1–Fe2–O4	102.10 (6)
O1–Fe1–O3	88.60 (6)	O1–Fe2–O5	90.13 (6)
O1–Fe1–N1	87.10 (6)	O1–Fe2–N4	86.86 (6)
O1–Fe1–N2	82.82 (6)	O1–Fe2–N5	83.69 (6)
O1–Fe1–N3	160.94 (6)	O1–Fe2–N6	161.32 (6)
O2–Fe1–O3	100.14 (7)	O4–Fe2–O5	96.96 (7)
O2–Fe1–N1	164.08 (7)	O4–Fe2–N4	164.93 (7)
O2–Fe1–N2	93.34 (7)	O4–Fe2–N5	91.29 (6)
O2–Fe1–N3	93.97 (7)	O4–Fe2–N6	95.90 (7)
O3–Fe1–N1	91.35 (7)	O5–Fe2–N4	95.08 (6)
O3–Fe1–N2	165.46 (6)	O5–Fe2–N5	170.59 (6)
O3–Fe1–N3	81.96 (7)	O5–Fe2–N6	82.74 (7)
N1–Fe1–N2	76.55 (7)	N4–Fe2–N5	77.54 (6)
N1–Fe1–N3	76.66 (6)	N4–Fe2–N6	76.66 (6)
N2–Fe1–N3	102.65 (7)	N5–Fe2–N6	100.97 (6)
Fe1–O1–C1	125.2 (1)	Fe2–O1–C1	125.8 (1)
Fe1–O2–C33	127.0 (2)	Fe2–O4–C35	127.1 (2)
Fe1–O3–C35	130.7 (2)	Fe2–O5–C33	132.4 (2)
Fe1–N1–C7	110.2 (1)	Fe2–N4–C20	110.8 (1)
Fe1–N1–C8	109.3 (1)	Fe2–N4–C21	108.4 (1)
Fe1–N1–C14	105.6 (1)	Fe2–N4–C27	105.9 (1)
Fe1–N2–C9	114.6 (1)	Fe2–N5–C22	123.2 (1)
Fe1–N2–C13	123.1 (2)	Fe2–N5–C26	112.7 (1)
Fe1–N3–C15	116.0 (1)	Fe2–N6–C28	115.1 (1)
Fe1–N3–C19	125.4 (2)	Fe2–N6–C32	126.4 (1)
Fe1–O1–Fe2	108.93 (6)		

[a] Estimated standard deviations in the least significant digits are given in parentheses.

(18) (a) By using the same approach, Suzuki et al. has reported the analogous $[Fe_2BPMP(OAc)_2]BF_4$ and $[Fe_2BPMP(OBz)_2]BF_4$ complexes in the paper: Suzuki, M.; Uehara, A.; Oshio, H.; Endo, K.; Yanaga, M.; Kida, S.; Saito, K. *Bull. Chem. Soc. Jpn.* **1987**, *60*, 3547–3555. (b) Suzuki, M.; Kanatomi, H.; Murase, I. *Chem. Lett., Chem. Soc. Jpn.* **1981**, 1745–1748.

(19) Borovik, A. S.; Que, L., Jr.; Papaefthymiou, V.; Münck, E.; Taylor, L. F.; Anderson, O. P. *J. Am. Chem. Soc.* **1988**, *110*, 1986–1988.

(20) *International Tables for X-ray Crystallography*; Kynoch Press: Birmingham, England, 1969; Vol. IV, pp 55, 99, 149.

refinement on F was carried out by alternately refining the cation or the anions plus solvent molecules until the largest shift/esd ratio was equal to 0.02. In the final ΔF map, the highest peaks were located near the partially occupied CH_2Cl_2 solvate positions.

The final fractional atomic coordinates for **1** are contained in Table S1, while bond lengths and angles for the dinuclear complex cation are reported in Table II. A complete listing of bond lengths and angles and thermal parameters is found in the supplementary material. The structure of the cation is shown in Figure 1, together with the numbering scheme for the complex.

Physical Methods. Visible spectra of the complexes in acetonitrile were obtained by using Hewlett Packard 8451A diode array and Cary 219 spectrophotometers. All samples were prepared under nitrogen.

^1H NMR spectra of the dinuclear metal complexes were obtained on an IBM AF-300 NMR spectrometer. Samples with concentrations ranging from 5–10 mM required 5000 scans to obtain adequate signal-to-noise ratios. For T_1 determinations, $t_{FID} + t_{delay}$ was set to 300 ms to ensure complete relaxation of the paramagnetically shifted resonances between pulses. The spectra were obtained with modifications of the inversion-recovery pulse sequence $(180° - \tau - 90° - t_{FID} - t_{delay})_n$ by using quadrature phase cycling. The 180° pulse (ca. 10 μs) was replaced by a $90°_x$–$240°_y$–$90°_x$ composite pulse to provide more effective inversion over the ca. ±40 kHz spectral range.[21] A linear base line correction was applied to sections of the spectrum from which peak positions, widths, and amplitudes were determined by using the spectral simulation program NMCCAP of the Nicolet NMR software package. Each spectrum was simulated in order to leave a difference (obs − calc) spectrum with no visually apparent peak-like features. The intensities of the various peaks as determined by NMCCAP were fit by a nonlinear least-squares program to the equation[22]

$$I(\tau) = I_\infty[1 - (1 + w)\exp(-\tau/T_1)]$$

Three parameters (T_1, I_∞ and w) were allowed to vary. The parameter w generally refined to between 0.70 and 1.00 (the latter value indicates complete population inversion by the 180° pulse).

EPR spectra were obtained at X-band with a Varian E-109 spectrometer equipped with an Oxford Instruments ESR-10 liquid helium cryostat; a Varian E-236 bimodal cavity was used for both perpendicular and parallel B_1 mode studies. Samples were prepared under nitrogen, with all solvents distilled prior to use and degassed by five freeze–pump–thaw cycles. The Mössbauer spectrometer was of the constant acceleration type, and the isomer shifts are relative to iron metal at 300 K.

Results and Discussion

Synthesis. To model the diferrous centers found in hemerythrin, methane monooxygenase, and ribonucleotide reductase, we have synthesized complexes with (μ-phenoxo)bis(μ-carboxylato)diiron(II) cores based on the dinucleating ligand HBPMP. The synthesis of $[Fe^{II}_2BPMP(OPr)_2]BPh_4$ (**1**) and $[Fe^{II}_2BPMP(OBz)_2]BPh_4$ (**2**) is readily achieved by reacting 1 equiv of the dinucleating ligand with 2 equiv of $Fe(BF_4)_2$ and the sodium salt of the appropriate carboxylic acid in methanol, followed by metathesis by $NaBPh_4$. The resulting solids afford satisfactory elemental analyses after recrystallization.

The corresponding $Fe^{II}Zn^{II}$ and $Fe^{II}Ga^{III}$ complexes were obtained for spectroscopic comparisons. The synthesis of $[Fe^{II}Zn^{II}BPMP(OPr)_2]BPh_4$ (**3**) could not be achieved directly from its components due to the formation of homodinuclear complexes, even by the sequential addition strategy successfully employed in the synthesis of $[M^{II}M'^{III}BPMP(O_2CR)_2]^{2+}$ complexes[19] because of the lower affinity of divalent ions for the phenolate ligand. **3** was thus synthesized by the reduction of the corresponding $Fe^{III}Zn^{II}$ complex in CH_3CN; NMR solution studies of the resultant complex indicate that metal site scrambling occurs slowly in CH_3CN, and most solution studies should be carried out within a few hours of complex dissolution. $[Fe^{II}Ga^{III}BPMP(OPr)_2](BPh_4)$ (**4**) was obtained by the sequential addition strategy reported previously.[19]

Solid-State Structure of $[Fe^{II}_2BPMP(OPr)_2](BPh_4)\cdot 0.8CH_2Cl_2$ (1). The structure of **1** (Figure 1) shows two iron centers bridged by the phenolate oxygen atom of $BPMP^-$ and by two propionate ligands. This triply bridged core structure increasingly appears to be a thermodynamically favored structural unit and has been found for a variety of structurally characterized dinuclear metal complexes including homobimetallic complexes containing $Fe(III)_2$,[7,23-25] $Fe^{II}Fe^{III}$,[19,26] $Fe(II)_2$,[15,16] $Mn(III)_2$,[27] $V(III)_2$,[28] $Mo(III)_2$,[29] and $Ru(III)_2$[30] units and heterobimetallic complexes with $Co^{II}Cr^{III}$,[31] $Fe^{II}Cr^{III}$,[32] $Fe^{III}Mn^{III}$,[33] and $Fe^{III}Zn^{II}$[19] centers.

Table III. Comparisons of the Diiron(II) Complexes

property	1[a]	5[b]	6[c]
Fe-μ-OR (Å)	2.052 (1)	1.987 (8)	2.129 (9)
	2.062 (1)		2.168 (8)
Fe-μ-O,O'-RCO_2 (Å)	2.09	2.13	2.11
Fe···Fe (Å)	3.348 (1)	3.32 (1)	3.585 (4)
Fe–O–Fe (deg)	108.93 (6)	113.2 (2)	113.1 (4)
J (cm^{-1}, $\mathcal{H} = JS_1\cdot S_2$)	n.d.	26.2	n.d.
EPR	$g \sim 16$	silent	$g \sim 16$
Mössbauer δ (mm/s)	1.20	1.16, 1.15	1.25, 1.26
ΔE_Q (mm/s)	2.72	2.83, 2.76	3.30, 2.56

[a] This work. [b] References 15a and b. [c] Reference 16.

The core dimensions of **1** are compared in Table III to those of $[Fe_2(OH)(OAc)_2(Me_3TACN)_2]ClO_4$ (**5**)[15] and $[Fe_2(BIPhMe)_2(HCO_2)_4]$ (**6**),[16] the two other structurally characterized tribridged diferrous complexes. The Fe–μ-O bonds in **1** at 2.052 (1) and 2.062 (1) Å are intermediate between those of **5** and **6**, consistent with the intermediate basicity of the phenolate relative to those of hydroxide and formate. The O,O'-bridging carboxylates, on the other hand, are coordinated more strongly in **1** (average $Fe-O_{carboxylate}$ = 2.09 Å) than in **5** (average $Fe-O_{carboxylate}$ = 2.13 Å) and **6** (average $Fe-O_{carboxylate}$ = 2.11 Å), reflecting the relative Lewis acidities of the ferrous centers in the three complexes. In **1** and **6**, the bidentate carboxylates bridge asymmetrically. While the asymmetry in **6** is due to the presence of five-coordinate and six-coordinate iron(II),[16] that observed for **1** appears characteristic of complexes of such dinucleating ligands.[19,25] The Fe–Fe distances in **1** and **5** are comparable at 3.348 (1) and 3.32 (1) Å, respectively, and similar to the metal–metal separations in other tribridged complexes with a μ-phenoxo or μ-hydroxo group,[19,23-25] but significantly shorter than that found for **6** (3.585 (4) Å), which is the only known tribridged diiron complex with an O,O-carboxylato bridge. The Fe1–O–Fe2 angle of 108.93 (6)° for **1** is smaller than the ca. 113° angles found for **5** and **6**.

The iron–ligand bond lengths found for **1** are those expected from a comparison of other ferrous complexes. The Fe1–O1 and

(21) Levitt, M. H. *J. Magn. Reson.* **1983**, *51*, 128–133.
(22) Levy, G.; Peat, I. *J. Magn. Reson.* **1975**, *18*, 500.
(23) Armstrong, W. H.; Lippard, S. J. *J. Am. Chem. Soc.* **1984**, *106*, 4632–4633.
(24) Murch, B. P. Ph.D. Thesis, Cornell University, 1987.
(25) Murch, B. P.; Bradley, F. C.; Que, L., Jr. *J. Am. Chem. Soc.* **1986**, *108*, 5027–5028.
(26) Mashuta, M. S.; Webb, R. J.; Oberhausen, K. J.; Richardson, J. F.; Buchanan, R. M.; Hendrickson, D. N. *J. Am. Chem. Soc.* **1989**, *111*, 2745–2746.
(27) (a) Wieghardt, K.; Bossek, U.; Ventur, D.; Weiss, J. *J. Chem. Soc., Chem. Commun.* **1985**, 347–349. (b) Wieghardt, K.; Bossek, U.; Zsolnai, L.; Huttner, G.; Blondin, G.; Girerd, J.-J.; Babonneau, F. *J. Chem. Soc., Chem. Commun.* **1987**, 651–653. (c) Sheats, J. E.; Czernuszewicz, R. S.; Dismukes, G. C.; Rheingold, A. L.; Petrouleas, V.; Stubbe, J.; Armstrong, W. H.; Beer, R. H.; Lippard, S. J. *J. Am. Chem. Soc.* **1987**, *109*, 1435–1444. (d) Diril, H.; Chang, H.-R.; Zhang, X.; Larsen, S. R.; Potenza, J. A.; Pierpont, C. G.; Schugar, H. J.; Isied, S. S.; Hendrickson, D. N. *J. Am. Chem. Soc.* **1987**, *109*, 6207–6208. (e) Suzuki, M.; Mikuriya, M.; Murata, S.; Uehara, A.; Oshio, H.; Kida, S.; Saito, K. *Bull. Chem. Soc. Jpn.* **1987**, *60*, 4305–4312. (f) Menage, S.; Girerd, J.-J.; Gleizes, A. *J. Chem. Soc., Chem. Commun.* **1988**, 431–432.
(28) Wieghardt, K.; Köppen, M.; Nuber, B.; Weiss, J. *J. Chem. Soc., Chem. Commun.* **1986**, 1530–1532.
(29) Neves, A.; Bossek, U.; Wieghardt, K.; Nuber, B.; Weiss, J. *Angew. Chem., Int. Ed. Engl.* **1988**, *27*, 685–687.
(30) (a) Sasaki, Y.; Suzuki, M.; Tokiwa, A.; Ebihara, M.; Yamaguchi, T.; Kabuto, C.; Ito, T. *J. Am. Chem. Soc.* **1988**, *110*, 6251–6252. (b) Neubold, P.; Wieghardt, K.; Nuber, B.; Weiss, J. *Inorg. Chem.* **1989**, *28*, 459–467.
(31) Chaudhuri, P.; Winter, M.; Küppers, H.-J.; Wieghardt, K.; Nuber, B.; Weiss, J. *Inorg. Chem.* **1987**, *26*, 3302–3310.
(32) Chaudhuri, P.; Winter, M.; Küppers, H.; Wieghardt, K.; Nuber, B.; Weiss, J. *Inorg. Chem.* **1987**, *26*, 3302–3310.
(33) Bossek, U.; Weyhermüller, T.; Wieghardt, K.; Bonvoisin, J.; Girerd, J. J. *J. Chem. Soc., Chem. Commun.* **1989**, 633–636.

Table IV. NMR Properties of the Dinuclear Complexes with Proposed Assignments[a]

	1[b]	3[b]	4[c]
BPMP CH_2	181 (2.9), 76 (3.1), 74 (0.8), 74 (2.6), −14 (1.0), −27 (1.6)	190 (2.8), 82 (3.3), 81 (2.6), 79 (0.8), 25.5, −21 (1.3)	232 (3.9), 122 (4.3), 97 (4.4), 42 (1.0), 33 (1.0)
pyridine *o*-H[d]	171 (0.9), 147 (0.9)	159 (0.9), 147 (0.9)	178 (1.0), 106 (1.0)
pyridine *m*-H	62 (12), 42 (16), 42 (12), 27 (13)	55 (15), 47 (16), 44 (15), 31 (12)	62 (17), 52 (20) 46 (24), 45 (17)
pyridine *p*-H	11 (29)		
phenolate *m*-H	26 (14)[e]	22 (43),[e] 14.5 (22)[e]	19 (21)
phenolate *p*-CH_3	33 (65)	19.5 (105)	9 (148)
propionate CH_2[f]	51 (4.8), 39 (4.7)	36 (9.5), 28 (9.1), 18 (6.8), 15 (7.7)	36 (13), 19.5 (12), 19 (21), 16 (13)
propionate CH_3	12 (8)		
acetate CH_3[g]	50	33, 18	

[a] T_1 values are indicated in parentheses. Assignments are proposed based on chemical shifts, T_1 values, integrations, and atom substitutions (in selected cases). Protons with shifts near the diamagnetic region are difficult to assign at present and await a more detailed NMR investigation. [b] In $CDCl_3$. [c] In acetone-d_6. [d] T_1 values are also consistent with a BPMP CH_2 assignment, but these protons are tentatively assigned to the pyridine ortho protons on the basis of chemical shifts. [e] Assigned by deuterium substitution. [f] Assigned by comparison with corresponding acetate complexes. [g] Methyl resonances of corresponding acetate complexes.

Fe2–O1 bonds at 2.062 (1) and 2.052 (1) Å, respectively, are somewhat shorter than that found for the Fe(II)–O(phenolate) bond in the mixed valence $[Fe_2BPMP(OPr)_2](BPh_4)_2$, 2.090 (2) Å.[19] This is not unexpected, since the Fe(II)–μ-O bond in the latter complex would be weakened by the presence of the stronger Fe(III)–μ-O interaction. The average Fe(II)–O value of 2.08 Å for **1** matches well with the 2.08 and 2.06 Å values observed for **5**[15] and $[Cr^{III}Fe^{II}(OH)(OAc)_2(Me_3TACN)_2]^{2+}$,[32] respectively. The average Fe(II)–N value of 2.22 Å is intermediate between the 2.17 Å value found for the Fe(II) site in $[Fe_2BPMP(OPr)_2](BPh_4)_2$ and the 2.29 Å value for **5**.

Complex **1** does not exhibit any crystallographically imposed symmetry, but there is a pseudo 2-fold axis about the C1–O1 bond. The BPMP ligand adopts a conformation that is similar to those observed in structures of other BPMP complexes.[19] The phenyl ring of the $BPMP^-$ ligand is twisted relative to the Fe1–O1–Fe2 plane, resulting in a dihedral angle of 48° between the plane defined by the C1–C6 carbon atoms of the phenolate ring and the Fe1–O1–Fe2 plane. This twist of the phenolate ring relative to the Fe–O–Fe plane is also observed in $[Fe^{II}Fe^{III}BPMP(OPr)_2](BPh_4)_2$ and $(Me_4N)[Fe^{III}_2HXTA(OAc)_2]$ with dihedral angles of 53° and 40°, respectively.[19,25]

Visible Spectra. **1** exhibits a visible absorption maximum at 422 nm (ϵ 2300 M^{-1} cm^{-1}). This feature shifts to 441 nm upon substitution of propionate with the less basic benzoate in **2**, suggesting that it is a metal-to-ligand charge-transfer transition, specifically Fe(II)-to-pyridine. Similar features are observed for the $Fe^{II}Zn^{II}$ and $Fe^{II}Ga^{III}$ derivatives at 448 and 387 nm, respectively.

NMR Properties. The ^1H NMR spectra of **1**, **3**, and **4** consist of relatively sharp resonances that span over 200 ppm in chemical shift (Figure 2 and Table IV). The high resolution and the relatively narrow line widths observed in the spectra are as expected for these high-spin Fe(II) complexes.[34] The spectrum of **1** exhibits effective 2-fold symmetry with essentially no features in the diamagnetic region except for the BPh_4 and residual solvent protons. The spectra of **3** and **4**, on the other hand, exhibit paramagnetically shifted peaks which are associated with the Fe(II) half of the molecule and a number of features in the 0–20-ppm region which are associated with the Zn(II) or Ga(III) half and are shifted due to the dipolar effects of the Fe(II) center. Many of the paramagnetically shifted features can be tentatively assigned on the basis of chemical shift comparisons with suitable model compounds, integrations, atom substitution experiments, and T_1 values. The T_1 values, which are proportional to the inverse sixth power of the Fe(II)–H distance, subdivide the ligand resonances into three categories: (1) those with T_1 values of <4 ms which correspond to Fe(II)–H distances of <4 Å, i.e., the CH_2 groups of $BPMP^-$ and the pyridine ortho protons; (2) those with T_1 values of 4–25 ms which correspond to Fe(II)–H distances of 4–5.5 Å, i.e., pyridine and phenolate meta protons; and (3) those with T_1 values >25 ms which correspond to protons at distances >5.5 Å from the metal center. A detailed NMR investigation of these complexes is in progress and will be reported in a subsequent paper.

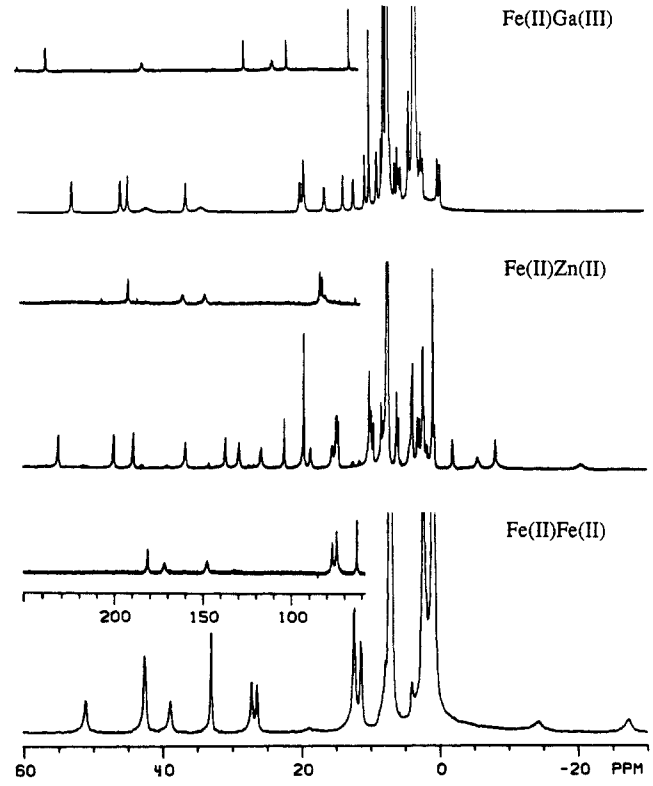

Figure 2. ^1H NMR spectra of $[MM'BPMP(OPr)_2](BPh_4)_n$ at 300 K. The small shaded features in the spectrum of the FeZn complex represent <5% contamination of the Fe_2 complex.

A glance at Figure 2, however, provides some useful chemical insights. We note that traces of **1** can be detected in the spectrum of **3**, indicating that some disproportionation of **3** into homodinuclear complexes occurs. On the basis of relative areas of the peaks, we estimate that there is <5% of **1** in this sample of **3**, and the amount of **1** increases upon prolonged standing in solution. **4**, on the other hand, is quite stable and shows no evidence for decomposition; this is undoubtedly due to the affinity of the Ga(III) for the phenolate in the BPMP ligand.

A comparison of the data in Table IV indicates that the replacement of an Fe(II) ion in **1** with Ga(III) elicits a larger structural change in the dinuclear complex than with Zn(II). We suggest that the spectral differences arise from the expected greater

(34) Bertini, I.; Luchinat, C. *NMR of Paramagnetic Molecules in Biological Systems*; Benjamin Cummings: Menlo Park, CA, 1986.

Table V. Temperature Dependence of the Mössbauer Parameters for Both Iron Sites of Polycrystalline **1**

	Fe1			Fe2		
T (K)	δ^a	$\Delta E_Q{}^b$	Γ^c	δ^a	$\Delta E_Q{}^b$	Γ^c
4.2	1.21	2.87	0.27	1.22	2.52	0.37
55.0	1.21	2.86	0.28	1.22	2.49	0.36
93.0	1.20	2.79	0.29	1.21	2.31	0.39
113.0	1.19	2.74	0.32	1.20	2.12	0.40
153.0	1.17	2.62	0.32	1.18	1.92	0.33
203.0	1.145	2.45	0.29	1.15	1.79	0.27

[a] In mm/s relative to Fe metal at 300 K. [b] In mm/s; signs of ΔE_Q are positive. [c] FWHM in mm/s.

affinity of Ga(III) for the bridging phenolate which should weaken the basicity of the phenolate toward the Fe(II) in **4** and in turn strengthen the Fe(II)–pyridine interactions. One would thus expect larger shifts for the pyridine protons in **4** relative to those in **1** and **3**, and this is indeed observed. For example, the average pyridine meta-H shift is 44 ppm for both **1** and **3** and 52 ppm for **4**.

The shifts of the bridging phenolate protons, not surprisingly, also respond accordingly. The meta-H and para-CH_3 resonances in **1** are found at 27 and 32 ppm, respectively. Replacement of one Fe(II) with Zn(II) to generate **3** results in decreased shifts for the meta-H (14.5 and 22 ppm) and the para-CH_3 protons (19.5 ppm) due to diminished delocalization of unpaired spin density from only one Fe(II) center. Furthermore, the two meta-H protons become distinct because of the lack of 2-fold symmetry. Replacement of Zn(II) with the more Lewis acidic Ga(III) to yield **4** diminishes the *p*-CH_3 shift to 9 ppm, a direct consequence of the decreased basicity of the bridging phenolate toward the Fe(II) as discussed earlier.

The shift behavior of the propionate CH_2 resonances in these complexes is also interesting; they have been assigned by comparison with the corresponding acetate complexes. They are found at 37 and 49 ppm in the $Fe(II)_2$ complex, compared to 15, 18, 28, and 36 ppm in the Fe(II)Zn(II) complex. The propionate CH_2 protons are diastereotopic; only two resonances are expected for the 2-fold symmetric **1**, while four are expected for **3**. Due to the asymmetric bridging mode observed for carboxylates in this family of dinuclear complexes, one carboxylate is more strongly associated with the Fe(II) and the other with the Zn(II). This difference in Fe(II)–ligand bonding will affect the extent of unpaired spin density delocalized onto the respective ligands. We thus attribute the more downfield shifted pair to the propionate that is coordinated more strongly to the Fe(II) center and the less downfield shifted pair to the propionate which is bound more tightly to the Zn(II) center and would thus have less unpaired density delocalized from the Fe(II). The propionate resonances in **4** are affected similarly.

Mössbauer Spectra. Mössbauer spectra of **1** as a polycrystalline solid are shown in Figure 3. The zero-field spectra exhibit, especially at higher temperature, two quadrupole doublets with a 1:1 area ratio. The two doublets have nearly the same isomer shifts, and the shifts are typical of high-spin ferrous centers in six-coordinate (O,N) environments. The quadrupole splittings of both sites depend quite strongly on the temperature, indicating that both sites have low-lying excited states which become populated at $T > 100$ K. Since the two sites have different ΔE_Q values and different temperature dependences for the ΔE_Q's, it follows that both sites have different orbital level splittings and thus experience distinct environments, in accord with the crystallographic results. Table V lists the results of fitting the zero-field spectra to two quadrupole doublets.

Spectra recorded at $T > 100$ K in an applied field of 6.0 T (data not shown) show that both sites have $\Delta E_Q > 0$. The low-temperature high field spectra are difficult to analyze for two reasons. First, the electronic spin relaxation rate is intermediate ($\approx 10^7$ s^{-1}) in the temperature range $4.2 < T < 100$ K. Secondly, the applied field spectra depend on a large number of unknowns (at least 16 parameters), and a successful data analysis requires information from complementary techniques.

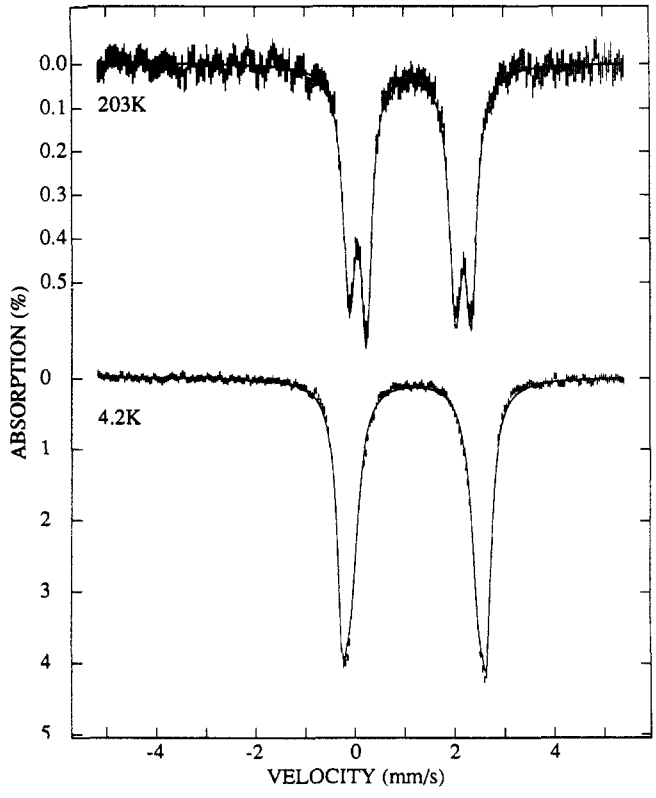

Figure 3. Mössbauer spectra of a polycrystalline sample of **1**. The solid lines are the results of the least-squares fitting two quadrupole doublets to the spectra. The parameters are quoted in Table V.

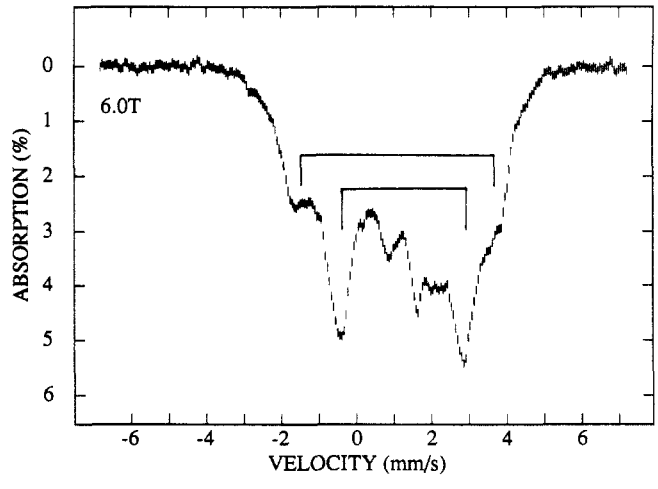

Figure 4. Low-temperature Mössbauer spectrum of **1**, recorded at 1.4 K in a 6.0 T parallel field. The brackets mark the outermost lines of the inequivalent Fe(II) sites. This identification is based on extensive computer simulations which account for the gross features of the spectra.

Figure 4 shows a spectrum recorded at $T = 1.4$ K in a 6.0 T parallel field. From a series of spectral simulations, we have drawn the following conclusions. The spectrum consists of a superposition of two distinct magnetic components; the outermost features of these subspectra are indicated by the brackets in Figure 4. The two sites are exchange-coupled, and the coupling is of the same order of magnitude as the zero-field splitting parameter D, i.e. $|J| < 15$ cm^{-1}. In order to analyze these data in more detail, we have started to study the high field spectra of the Fe(II) sites in the corresponding $Fe^{II}Zn^{II}$ and $Fe^{II}Ga^{III}$ complexes; from such studies one can obtain good estimates of the zero-field-splitting parameters and the magnetic hyperfine tensors to be used in the simulation of the spectra of the diferrous complex.

We have also examined spectra of **1** dissolved in CH_3CN. The zero-field spectra consist of one quadrupole doublet. The absorption lines, however, are broad (~0.55 mm/s FWHM) and

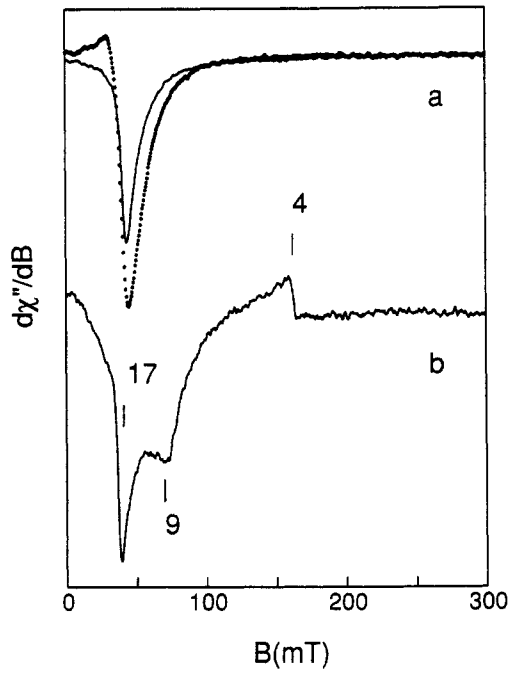

Figure 5. X-band EPR spectra of frozen solutions of (a) 5.0 mM **1** in DMF (—) and 5.0 mM **2** in CH_2Cl_2 (···) and (b) **3** in CH_2Cl_2 (contains <5% of **1**). Instrumental parameters: T = 3 K, microwave, 9.1 GHz at 2 μW (a) or 2 mW (b). Spectra of (a) are normalized for instrumental parameter differences and (b) is plotted on an arbitrary scale to show a spectral feature comparison. Frozen solutions of **1** give identical spectra in either DMF or CH_2Cl_2. The signal at g = 4 in (b) is due to a ferric impurity which is not fully suppressed.

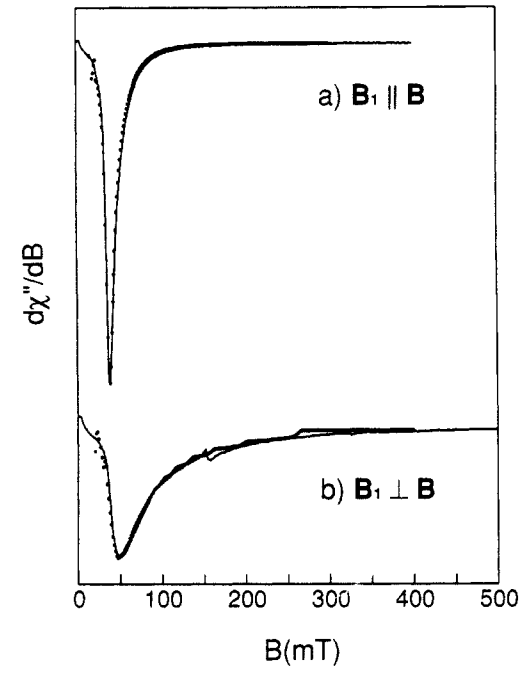

Figure 6. X-band EPR spectra (—) and simulations (···) of a frozen 5.0 mM solution of **1** in DMF at T = 3 K with (a) $\mathbf{B}_1 \parallel \mathbf{B}$ and (b) $\mathbf{B}_1 \perp \mathbf{B}$. Simulation parameters: S = 4, $\tilde{g}$ = 18, ground doublet, Δ° = 0.3 cm, $\sigma_\Delta \approx 0.5$ cm^{-1} where Δ° is the center of a spread in Δ values with width σ_Δ. Instrumental parameters: microwave frequency, 9.1 GHz at 0.2 mW; modulation, 100 kHz at 1 mTpp; gain, 2500; dB/dt, 2 mT/s.

non-Lorentzian, indicating a heterogeneous distribution of ΔE_Q values about a mean ΔE_Q which seems to be the average of the two values observed for the polycrystalline material.

EPR Studies. EPR spectroscopy is in general used to study complexes with half-integer electronic spin (Kramers systems). For an isolated Kramers doublet with **S** = 1/2, Zeeman interaction β**S**·**g**·**B**, and negligible hyperfine interactions, the quantization axis is along **g**·**B**. If the magnetic component of the microwave field, $\mathbf{B}_1$, is parallel to **B**, the effective microwave field $\mathbf{g}\cdot\mathbf{B}_1$ is parallel to the quantization axis no matter how the molecule is oriented relative to **B**. Since there are no $\Delta m_s = 0$ transitions between the levels of a Kramers doublet, no EPR signal is observed when the cavity is operated in parallel mode ($\mathbf{B}_1 \parallel \mathbf{B}$). Systems with integer spin, on the other hand, behave quite differently. One can observe transitions between levels which are separated at $B = 0$ by an energy gap Δ provided that $\Delta \leq h\nu$. For $B \neq 0$ the electronic quantization axis is determined by competition between the zero-field splitting (which produces Δ) and the Zeeman interaction. Since the driving term, $\beta\mathbf{S}\cdot\mathbf{g}\cdot\mathbf{B}_1$, consists only of the Zeeman interaction, the effective microwave field $\mathbf{g}\cdot\mathbf{B}_1$ and the quantization axis are in general not parallel, and EPR transitions can be observed both in parallel and perpendicular mode. Moreover, the levels between which the transition occurs can have components with the same m_s quantum number and the transition thus can have a $\Delta m_s = 0$ contribution.

Complexes **1** and **2** exhibit intense X-band EPR signals at approximately 50 mT applied field (Figure 5a). Similarly, **3** and **4** which contain mononuclear Fe(II) sites show EPR signals at low field (a spectrum of **3** is shown in Figure 5b), which are comparable to those observed for high-spin ferrous complexes such as Fe^{II}(EDTA)[35] and deoxymyoglobin.[36] The spectra of **1**–**4** all have significantly enhanced intensity in parallel mode relative to perpendicular mode (Figure 6). The signals from **3** and **4**, however, are significantly broader and much less intense than those of **1** and **2**. Indeed the signal amplitudes of **1** and **2** are approximately two orders of magnitude larger than those observed for **3** and **4**. As an illustration, the EPR spectrum of **3** (Figure 5b) shows a contaminating amount of **1**, which dominates the low field region. However, the contaminating amount of **1** in **3** can be estimated from NMR measurements of the same sample to be only <5%.

In parallel mode, the spectrum of **1** exhibits a sharp valley at g = 17 (Figure 6a). The temperature dependence of the signal shows that it results from a ground doublet; the signal intensity at 2 K is twice that at 4 K. The resonance condition for such signals is

$$(h\nu)^2 = \Delta^2 + (\tilde{g}\beta B)^2 \qquad (1)$$

where Δ is the splitting of the quasi-degenerate doublet in zero field and $\tilde{g}$ is an effective g value of the doublet.[35] We have simulated the spectra of **1** (Figure 6) according to the formalism described by Hendrich and Debrunner,[35] and there is excellent agreement between the experimental and simulated spectra in both parallel and perpendicular mode. The ratio of signal intensities in parallel and perpendicular modes (zero-to-valley) is 2.7, which is typical for many integer spin systems.[35] Our simulations assume that strain dominates the line width and that this strain is describable by a distribution of Δ values, centered at Δ° = 0.3 cm^{-1}. The spectra have finite intensities (χ'') at $B = 0$; half of the sites have $\Delta > 0.3$ cm^{-1} and are not observed at X-band.

The EPR results on **1** are very similar to those observed for the azide complex of deoxyhemerythrin (deoxyHrN_3); indeed the spectra of the two species are virtually indistinguishable with one important exception: for samples of equal concentration, the intensity of the signal from **1** is only 25% of that observed for deoxyHrN_3.

The low-lying energy levels of two exchange coupled ferrous ions ($\mathbf{S}_1 = \mathbf{S}_2 = 2$) may be described by

$$\mathcal{H} = J\mathbf{S}_1\cdot\mathbf{S}_2 + \sum_{i=1}^{2}[D_i(S_{zi}^2 - 2) + E_i(S_{xi}^2 - S_{yi}^2) + \beta\mathbf{S}_i\cdot\mathbf{g}_i\cdot\mathbf{B}] \qquad (2)$$

where D_i and E_i are the zero-field-splitting parameters of the two ferrous ions. The Mössbauer spectra show that the two sites are distinct, and we anticipate therefore that their zero-field splitting

(35) Hendrich, M. P.; Debrunner, P. G. *Biophys. J.* **1989**, *56*, 489–506.
(36) Hendrich, M. P.; Debrunner, P. G. *J. Magn. Reson.* **1989**, *78*, 133–141.

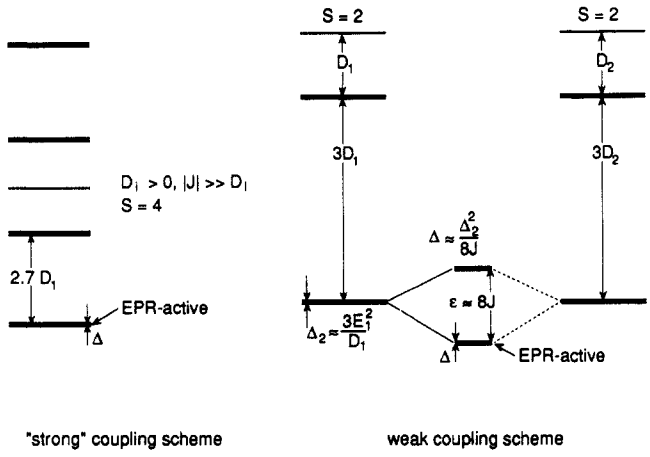

Figure 7. Limiting coupling schemes compatible with the EPR data for **1**. Equation 1 defines Δ, the splitting of the EPR-active doublet in zero field.

parameters differ. Moreover, the principal axis frames of the two zero-field splitting tensors need not coincide. Currently, we are not able to determine all the unknowns of eq 2. We can, however, specify two limiting schemes compatible with the EPR data (Figure 7). Both schemes require ferromagnetic coupling; for simplicity we have assumed that all tensors of eq 2 are the same for both sites. The strong coupling scheme requires that $D_i > 0$ and $|J| \gg D_i$. For this case, the observed resonance at $g = 17$ arises from transitions between the approximate $|0\rangle$ and $|1^-\rangle = (|+1\rangle - |-1\rangle)/\sqrt{2}$ states of an $S = 4$ multiplet, where $|m\rangle$ designates the $|S = 4, m\rangle$ eigenstates. In the weak coupling scheme, $|J| < |D_i|/3$ the four $|2^\pm\rangle = (|+2\rangle \pm |-2\rangle)/\sqrt{2}$ sublevels of the two ferrous ions combine to form a quartet which splits by the exchange interaction into two quasi-degenerate doublets. For ferromagnetic coupling, the lower doublet is EPR-active, whereas the upper doublet is EPR-silent. The temperature dependence of the resonance at $g = 17$ suggests that, in the weak coupling scheme, the EPR-silent doublet is roughly 10 cm^{-1} above the ground doublet. Although the spectra of Figure 6 were simulated in the strong coupling scheme, both schemes are compatible with the limited information available. The simulations give the result that $\tilde{g} = 18$, from which we obtain $g_{i_{zz}} = 2.3$ if $D_i < 0$ or $g_{i_{yy}} = 2.3$ if $D_i > 0$. We wish to stress that simulations in the framework of an $S = 2$ spin Hamiltonian,[35] i.e., assuming uncoupled sites, not only failed to produce the correct lineshapes but also yielded signal intensities substantially below those observed for complex **1**.

The EPR data contain considerably more information than we have specified here. For instance, certain orientations of the zero-field-splitting tensors of eq 2 can be ruled out. We have collected many Mössbauer spectra, and we have obtained, in collaboration with Dr. E. P. Day, a large set of SQUID magnetization data for complex **1**. Despite considerable efforts, we have not yet been able to fit the entire data set with a unique set of spin Hamiltonian parameters.

Implications for the Diferrous States of Hemerythrin, Methane Monooxygenase, and Ribonucleotide Reductase. The most intriguing spectroscopic observations for the diferrous forms of the iron-oxo proteins are the presence of low field EPR signals for deoxyHrN_3,[9] MMO_{red},[10a] and $RRB2_{red}$.[11] These signals arise from transitions in integer spin manifolds because of their resonance positions and their enhanced intensities[35,37] when the microwave field $\mathbf{B}_1$ is applied parallel to the static field **B** compared to those observed for the more conventional $\mathbf{B}_1 \perp \mathbf{B}$ mode. In contrast, deoxyHr is EPR-silent due to the antiferromagnetic coupling of the two ferrous centers.[9,13]

There are three synthetic complexes that are related to the diferrous forms of the iron-oxo proteins. The first to be reported is complex **5**, which has a (μ-hydroxo)bis(μ-carboxylato)diiron(II) core, exhibits antiferromagnetic coupling ($J = 26$ cm^{-1}), and is thus EPR-silent.[15] These properties model those of deoxyHr well. The hydroxo bridge in **5** is replaced with phenoxo and *O,O*-carboxylato bridges in **1** and **6**,[16] respectively. Due to the weaker basicity of these ligands, such substitutions would be expeeted to weaken the metal–metal interaction (as manifested by the longer Fe–μ-O bonds) and thus decrease or eliminate the antiferromagnetic coupling between the ferrous centers. For the case of **1**, it is clear that the metal–metal interaction no longer affords a diamagnetic ground state. A similar conclusion is likely for **6** when its properties have been examined in detail. These complexes thus serve as models for the EPR active diiron(II) proteins. The transformation of the EPR-silent deoxyHr to an EPR-active deoxyHrN_3 is proposed to result from the protonation of the hydroxo bridge in deoxyHr by HN_3 upon binding.[9] Consistent with the observations on the model complexes, the conversion of a hydroxo bridge to an aqua bridge would be expected to remove the dominant antiferromagnetic coupling pathway and give rise to a complex with a paramagnetic ground state. The observation of similar signals for MMO_{red}[10a,37] and $RRB2_{red}$[11] suggests that the iron centers in these enzymes are bridged by similarly poor mediators of antiferromagnetic coupling. This difference between deoxyHr which binds O_2 reversibly and the other two proteins which activate O_2 may be one clue toward unraveling the puzzle of how nature tunes active sites to serve the different functions observed.

Acknowledgment. We thank Professor J. D. Britton for his generous help in solving the crystal structure. This work has been supported by the National Institutes of Health through Grants GM-38767 (L.Q.) and GM-22701 (E.M.), postdoctoral fellowships for A.S.B. (GM-11533) and M.P.H. (GM-12996), and a predoctoral traineeship for T.R.H. (GM-08277). We are also grateful for a NATO travel Grant 890146 for V.P.

Supplementary Material Available: Tables of atomic positional and thermal parameters and complete bond lengths and bond angles for **1** (15 pages). Ordering information is given on any current masthead page.

(37) Hendrich, M. P.; Münck, E.; Fox, B. G.; Lipscomb, J. D. *J. Am. Chem. Soc.* In press.